Bulgarian Chemical Communications, Volume 47, Special Issue D (pp. 82 – 88) 2015

Effect of surface modification agent and calcination process on the preparation of the hydrophobic magnetic silica aerogels by ambient pressure drying method

L. Amirkhani[1], J. Moghaddas[1*], H. Jafarizadeh [1]

[1]*Faculty of Chemical Engineering, Sahand University of Technology, Tabriz, Iran*

Received June 26, 2015, Revised September 10, 2015

Silica aerogel-iron oxide nanocomposites have been synthesized with sodium silicate precursor, iron oxide nanoparticles and ambient pressure drying method in this research successfully. For composite synthesis cogelation of the matrix precursor and the nanoparticles suspension method were used. Trimethylchlorosilane (TMCS) and hexamethyldisilazane (HMDZ) as modification agents were used to synthesize magnetic silica aerogel nanocomposite and their effects were studied. The properties of nanocomposites were determined by XRD, BET, VSM, AAS, FTIR, TEM and SEM methods. The results showed that by HMDZmodification agent, the magnetic and physical properties of iron oxide nanoparticles in silica matrix were retained. The XRD patterns proved the existence of magnetite in nanocomposite that was oxidized to maghemite after heating in 500˚C for 2 hr. The effect of iron oxide nanoparticles content also were studied and the results indicated that the density and specific surface area of the aerogels were increased with increasing the iron oxide amount.

Keywords: Silica aerogel, Iron oxide, Magnetic, Ambient pressure drying, Sodium silicate.

INTRODUCTION

Magnetic zero-dimensional nanoparticles especially magnetite (Fe_3O_4) and maghemite (γ-Fe_2O_3) have very important application in many technological area such as catalysts, sensors, nuclear waste separation, biotechnology/ biomedical and magnetic recording systems [1-3]. But applications of these fine particles usually are difficult because of their tending to aggregation and chemically active natures that causes they become oxidized in air easily. One method to solve these problems is coating nanoparticles with inorganic layers such as carbon and silica [4, 5]. Continuous matrix such as silica aerogel also can be used to disperse iron nanoparticles [6, 7]. Silica aerogels and their composites has recently attracted so much considerations because of their unusual properties such as very low density, high porosity, high specific surface area, low dielectric constant and excellent heat insulation value. Aerogels are synthesized by sol-gel method and the liquid of the gels must be exit by special drying method so that the solid structure are retained. If the gels are dried in ambient pressure and temperature, they lost their porosity because the effects of the capillary forces and in that condition the xerogels are formed. Supercritical drying is the usual method to synthesize aerogel and their composites. But this method is dangerous and very costly. By solvent exchange and surface modification of the gels, capillary stresses can be avoided and the shrinkages are decreased considerably [8, 9].

All the reported literature in the field of synthesis iron oxide- silica aerogel nanocomposites have used supercritical drying method and mainly silicon alkoxides such as tetramethyl orthosilicate (TMOS) and tetraethyl orthosilicate (TEOS) as silica precursors [3, 6, 7, 10-22]. Several materials such as iron acetylacetonate [10, 11, 13, 19, 20, 23, 24], iron acetate [19], iron nitrate [3, 6, 7, 14-16, 18, 25],iron carbonyl [12] and iron chloride [17, 22] were used as iron oxide precursor. Most of above mentioned studies used cogelation matrix precursor and the inorganic precursor to synthesis nanocomposite. In this method the creation favorite iron oxide phase is difficult. In this work, silica aerogel- iron oxide nanocomposite were synthesized by simple ambient pressure drying method and water glass as a cheap precursor for first time. Magnetite nanoparticles as iron precursor and co-gelation of the nanoparticles and the matrix precursor were used to synthesize nanocomposites. This approach offers the advantage of producing materials with a controllable loading of nanoparticles. Trimethylchlorosilane (TMCS) and hexamethyldisilazane (HMDZ) as modification agents were used to synthesize silica aerogel-iron oxide nanocomposite and their effects were studied. The effect of iron oxide content on nanocomposite properties was investigated. Moreover, synthesis steps were summarized in this work. The alcohol and solvent were added to hydrogel in one step,

To whom all correspondence should be sent:
E-mail: jafar.moghaddas@sut.ac.ir

therefore the synthesis was done in one day less than previous procedure [26].

EXPERIMENTAL

Chemicals and Characterization Tools

Iron oxide nanoparticles were prepared from US Research Nanomaterials Company. The other materials were purchased from Merck Company.
The bulk density of the nanocomposites was calculated using a microbalance scale, (10^{-5} g precision) and coulisse. The surface area was determined by Brunauer–Emmett–Teller (BET) method (BEL, JAPAN) from the amount of N_2 gas adsorbed at various partial pressures. The Fe content in the samples were determined using an atomic absorption spectrophotometer (AAS, GBC Avanta). Organic and inorganic bonds present in an composite samples were studied by Fourier transform infrared spectroscopy (FTIR) using a IR spectrophotometer (PU 9800, from Philips) which gave the information about the various chemical bonding such as –OH, Si–OH, Si–O–Si, Si– C, C–H and Fe–O. The pore structure and particle morphology were characterized by field emission scanning electron microscopy (FESEM, Mira 3-XMU) and transmission electron microscopy (TEM, Philips EM208). X-ray diffraction (XRD) measurements were performed at room temperature using a Bruker D8 advance X-ray diffractometer. Magnetic properties of samples were studied by a vibrating sample magnetometer (VSM, Daghigh Meghnatis Kashan Co.) at room temperature.

Synthesis

At first step for synthesis of silica aerogel- iron oxide nanocomposite, certain weight (0.02 -1 g) of iron oxide nanoparticles were dispersed in 20 cc deionized water by an ultrasonic mixer. The power of the mixer was 70 watt, and solutions were mixed for 1 hr. Then water glass was added to the mixture in 1 to 4 ratios. The solution pH was ~ 12 in this step. After well mixing, amberlite resin was used to exchange the ion Na^+ with H^+ and solution pH became 2-3. The hydrogel was prepared by controlled addition of the NH_4OH solution (1 M) to the obtained sol. In this step to prevent deposition of Fe_3O_4 nanoparticles, the pH was adjusted so that the gelation time was limited in 1 minute. The mixture was transferred to Teflon vessels in airtight condition and 50 °C temperature. After 3 hours aging, 2-propanol and n-hexane in equal ratios were added to hydrogel to exchange the solvent. This step lasted 14-20 hours. The modification agent was prepared by adding 25% TMCS or HMDZ in n-Hexane solution. After evacuation of propanol-hexane solution, surface modification agent was added to the gel. After 14-20 hours, the modification agent was extracted and the gels were dried. To drying, the gels were given in ambient temperature for one day. After that raising temperature program was applied from 50°C to 140°C slowly in one day.

Beside iron oxide- silica aerogel nanocomposite, iron oxide- silica xerogel nanocomposite and pure silica aerogel were synthesized and their properties were compared together. For synthesis xerogel nanocomposite, the first steps were done similar to iron oxide- silica aerogel synthesis, but after gelation, the gels were dried without any excess operation in 50°C. In pure silica aerogel, iron oxide nanoparticles weren't added to the sol and the other steps were repeated.

RESULTS AND DISCUSSION

Two modification agents, trimethylchlorosilane (TMCS) and hexamethyldisilazane (HMDZ), were used to change surface functional groups and prevent xerogel formation. The samples that were modified with HMDZ and TMCS will be named as "AH" and "AT" respectively.

Apparent color of AT nanocomposites was altered in modification step. In the first step, the formation gel was dark brown. This gel kept its color in solvent exchange step. But after modification, the gel became transparent and colorless and the final product became white (Figure 1 b, c, d). Surface modification of the silica gel with TMCS was done as below reaction [27]:

$$\equiv Si{-}OH + (CH_3)_3{-}Si{-}Cl \rightarrow \equiv Si{-}O{-}Si{-}(CH_3)_3 + HCl \quad (1)$$

It seems that after formation of HCl, the following reaction between iron oxide entrapped in the pores and hydrochloride acid was happened [28].

$$Fe_3O_4 + 8HCl \rightarrow FeCl_2 + 2FeCl_3 + 4H_2O \quad (2)$$

Thus resulting composition was iron chloride-silica aerogel nanocomposite and didn't have any respond to external magnetic field.

Apparent color of samples AH remained constant in all steps (Fig. 1 b′, c′, d′). Surface modification of the silica gel with HMDZ was done as below reaction [29]:

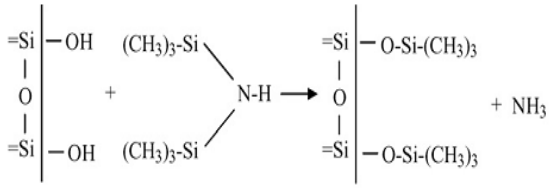

(3)

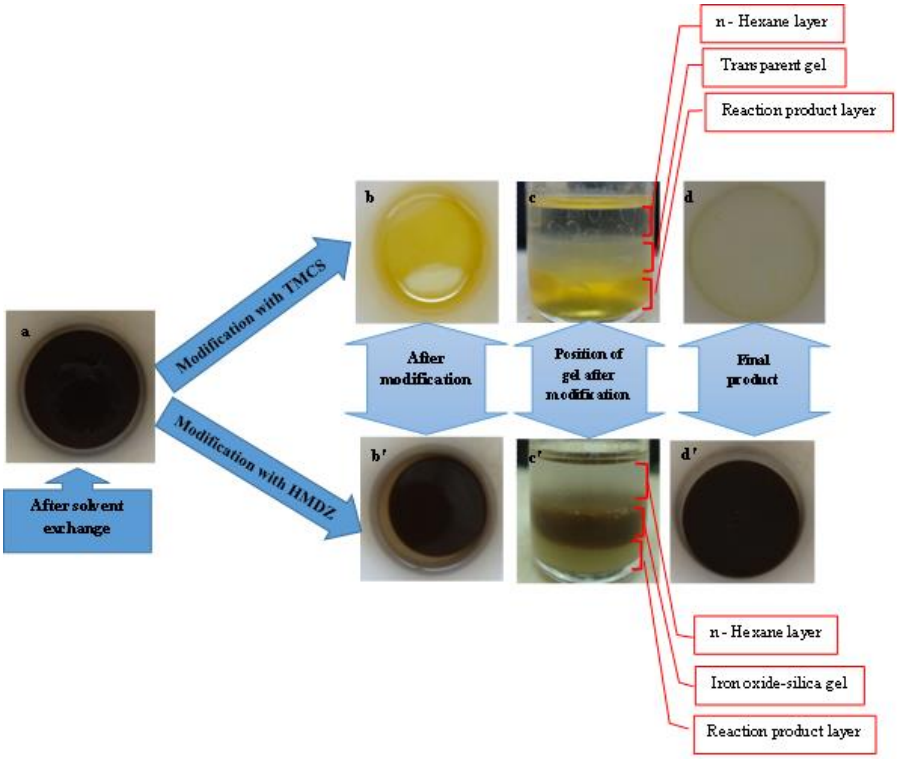

Fig. 1. Change in apparent color of iron oxide-silica gel in different steps (a) After solvent exchange; (b) and (b′) samples AT and AH after modification respectively; (c) and (c′) Position of gels after modification for samples AT and AH respectively; (d) and (d′) Final product of samples AT and AH respectively.

NH_3didn't react with Fe_3O_4 nanoparticles in modification step. Thus the structure and magnetic properties of Fe_3O_4 nanoparticles were retained. Resulting nanocomposites responded to external magnetic field strongly, so the main studies were done about samples AH.

Table 1 shows the effect of iron oxide initial weights on density and specific surface area of samples AH. Six initial weights of iron oxide nanoparticles (0.08, 0.1, 0.2, 0.5, 0.6 and 0.8 g) were examined and dispersed in 20ccdeionized water in first step of synthesis. The properties of pure iron oxide, silica aerogel and iron oxide-silica xerogel also were measured for comparison. The iron contents of samples were measured by atomic absorption spectroscopy (AAS). The measured Fe contents of samples were less than the additive amount in initial step. This was probably due to the leakage of a part of iron oxide nanoparticle at exchanging the solvent and surface modification steps from the pores. The other little part of iron oxide particles were attracted by ultrasonic mixer probe. As shown in table 1 the Fe content of sample AH with 0.5 g initial weight of iron oxide was less (5.74%) than its related xerogel (7.1%). Because in xerogel synthesis there wasn't any solvent exchange and modification steps, so the leakage of iron oxide nanoparticles was less than aerogel in these steps.

Table 1. The effect of initial weight of iron oxide on nanocomposite property.

Sample	Density (g/cm^3)	specific surface area (m^2/g)	Fe content (%)
Pure silica aerogel	0.12	589	0
AH (0.08)*	0.35	366.8	3.02
AH (0.1)	0.36	368.07	3.74
AH (0.2)	0.39	430.1	4.63
AH (0.5)	0.42	499	5.74
AH (0.6)	0.51	509	6.81
AH (0.8)	0.58	517	7.49
Iron oxide-silica xerogel (0.5)	2.2	521	7.1
Pure Fe_3O_4	5.1	82	100

* The numbers in parentheses are the initial amounts of iron oxide added to 20ccdeionized water in first step

The results showed that the density of samples AH were increased with increasing the iron oxide amount. The reaction between some of Fe_3O_4 nanoparticles and SiO_2 and formation of Fe-O-Si bonds led to decrease modification of SiO_2 with silylating agent. This increased volume shrinkage and density. The values of density for the samples AH were between 0.35-0.58 g/cm^3. For iron oxide-silica xerogel samples this value was 2.2 g/cm^3 and for pure silica aerogel was 0.12 g/cm^3. These results showed iron oxide- silica aerogel surface modification were done less than pure silica aerogel and more than xerogel samples. Thus the porosity of pure silica aerogels was larger than their composites. On the other hand the density of pure iron oxide was 5.1 g/cm^3 that reduced the density of composites. Figure 2 compares the apparent properties of sample AH with initial 0.5 g Fe_3O_4, its related xerogel and pure silica aerogel.

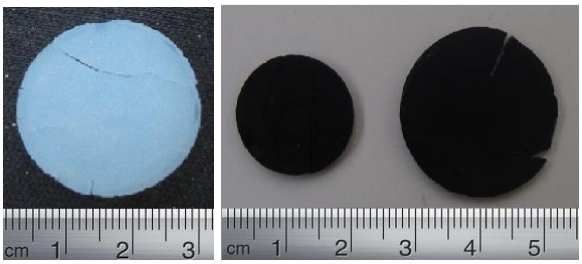

(a) (b) (c)

Fig. 2. Photographs of (a) pure silica aerogel; (b) magnetite-silica xerogel; (c) sample AH.

Two factors can affect on the nanocomposites specific surface area. The first factor isthe presence ofiron oxide nanoparticles with a low specific surface area that reduce the specific surface area ofthe compositesconsiderably. The specific surface area of bare magnetite was 82 m^2/g. Thus with iron oxide doping, the specific surface area of the composite was decreased respect to pure silica aerogel (Table 1). The second factor is the small pores volume in the dense structures leading to an increase in specific surface area of the composites. Increasing surface area with increasing the initial amount of iron oxide and decreasing the density in table 2 was for this reason. So with adding the appropriate amount of iron oxide, the properties of nanocomposites can be regulated.

Figure 3 shows the result of XRD patterns of the magnetite and sample AH with 0.5 g iron oxide before annealing. The pattern for sample AH had four characteristic peaks at 30.3˚ (220), 35.7˚ (311), 57.2˚ (511) and 62.7˚ (440) which was consistent with the standard pattern of Fe_3O_4 (00-019-0629). The broad peak between 20 and 30 degree in pattern of sample AH, was due to amorphous silica.This proved the existence of both amorphous silica and magnetite in nanocomposite before annealing.

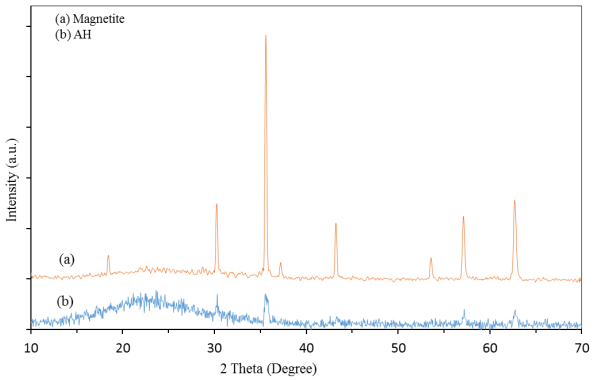

Fig. 3. The XRD pattern of (a) magnetite and (b) sample AH.

After annealing silica aerogel-magnetite nanocomposites in 500˚C for 2 hr their apparent color was changed from dark brown to light brown. Figure 4 shows the XRD patterns of the magnetite and sample AH after annealing. There were ten characteristic peaks at 24.2˚(210), 30.4˚(220), 33.3˚(310), 35.8˚(311), 41˚(321), 49.6˚(421), 54.2˚(430), 57.6˚(511), 62.5˚(440) and 64.1˚(441) for annealing magnetite and seven characteristic peaks for annealing sample AH at 22.6˚ (210), 30.4˚(220), 35.8˚(311), 43.4˚(400), 53.9˚(422), 57.5˚(511) and 63.1˚(440) that corresponded to Fe_2O_3 (00-039-1346).

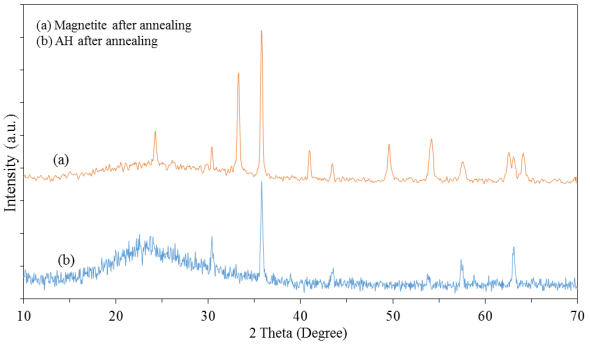

Fig. 4. The XRD pattern of (a) magnetite and (b) sample AHafter annealing in 500˚C for 2 hr.

These patterns showed that magnetite and sample AH were oxidized to maghemite and maghemite composite after heating in 500˚C for 2 hr. The broad amorphous silica peak was also seen in maghemite composite pattern. The result composite showed strong response to the external magnetic field that was also evidence of formation maghemite polymorph.

Figure 5 (a) and (b) shows the XRD pattern of the AT sample before and after heating in 500˚C for 2 hr respectively. Except of broad silica peak, any

other obvious peak wasn't seen. This showed that there wasn't any crystalline phase in silica structure that modified with TMCS.

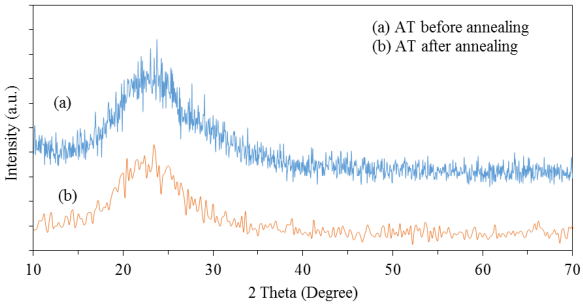

Fig. 5. The XRD pattern of sample AT: (a) before heating; (b) after heating in 500˚C for 2 hr.

Crystallite size (D) is calculated using the Debye-Scherer's formula: [30]

$$D = \frac{k\lambda}{\beta \cos\theta}, \quad (4)$$

Where β is the full width at half maximum (FWHM) of the corresponding XRD peak, k is a constant (~1), λ is X-ray wavelength and θ is the Bragg angle. Crystallite size of magnetite and sample AH before and after annealing were calculated by the Scherer formula and are shown in table 2. These results were confirmed nano crystallite size of structures.

Table 2. Crystallite size of samples magnetite and AH before and after annealing at 500˚C, calculated by the Scherrer formula.

sample	Crystallite size (nm)	
	Before annealing	After annealing
magnetite	42	34
AH	21	40

Figure 6 shows field emission scanning electron micrographs for sample AH with 0.5 g iron oxide in two resolution and pure silica aerogel. The structures were uniform and porous. Comparison between SEM images of pure silica aerogel and magnetic silica aerogel showed that, the porosity of composite was less than pure silica aerogel in agreement with the results of BET analysis. The figures also showed that the particles and the pores size is less than 50 nm in agreement with XRD results.

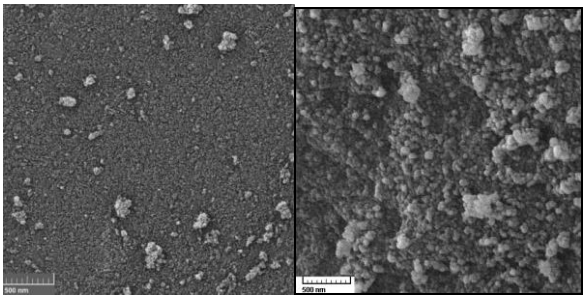

(a) (b)

Fig. 6. FESEM image of sample (a) AH with 0.5 g iron oxide(b) pure silica aerogel

The TEM images of the pure silica aerogel and sample AH were obtained at the scales of 25 nm and 20 nm, respectively (Figure 7).This analysis showed that iron oxide nanoparticles were surrounded by porous silica aerogel matrix. When the magnetic particles disperse in silica sol, the inherent affinity between the silica and iron molecules is caused the formation of silica gel around the iron oxide nanoparticles.

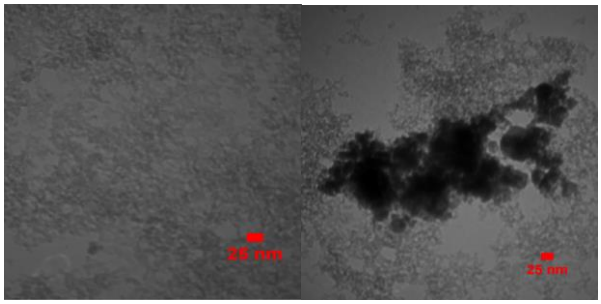

(a) (b)

Fig. 7. TEM images of (a) pure silica aerogel (b) iron oxide- silica aerogel composite

Magnetization curve in room temperature are shown in Figure 8 Measurements were obtained by the use of vibrating sample magnetometer (VSM) with maximum magnetic field of 10 kOe. This hysteresis loop shows 0.74 emu/g for Remanence magnetization (M_R), 6.65 emu/g for Saturation magnetization (M_S) and 97.5 Oe for coercive field (H_C).

The inset of Figure 8 is the magnetization curve of Fe_3O_4 nanoparticles that was measured in company. As could be seen from this picture, the value of M_S for nanoparticles is 60.45 emu/g. Decrease in saturation magnetization is possibly due to the non-magnetic silica aerogel layer that decreases surface moments. On the other hand in nanocomposite structure there is a little amount of ferromagnetic nanoparticles per unit weight [31].

Figure 9 shows the FTIR investigations of (a) sample AH and (b) sample AT. In Figure 9a the absorption peak at 585cm^{-1} is the characteristic

absorption of a Fe–O bond that confirm the presence of Fe_3O_4 nanoparticles [32]. This peak in Figure 9b is very weak that prove the reaction of Fe_3O_4 nanoparticles in this sample. The major peaks at around 3500 and1650 cm^{-1} are attributed to O-H bonding. In samples that were modified with TMCS these peaks are very weak. It shows that the surface modification with TMCS is more effective than HMDZ and the most of O-H groups are replaced with O-Si-$(CH_3)_3$.

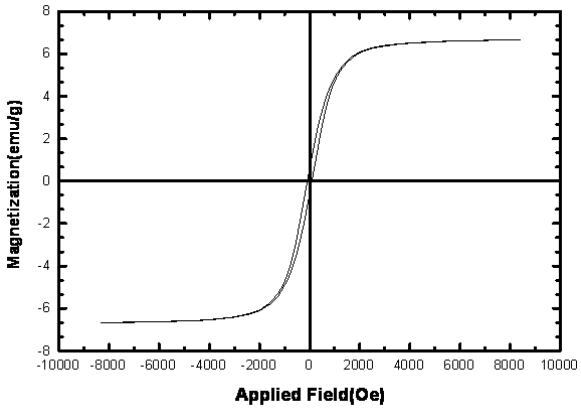

Fig. 8. Room temperature magnetization curve for iron oxide- silica aerogel nanocomposite. Inset figure is the magnetization curve of Fe_3O_4 nanoparticle

The peaks at around 2900 and 1450 cm^{-1} indicates to C-H bonds that were seen in two samples and were stronger in HMDZ samples due to two branches of $(CH_3)_3$ groups in this material. The peaks at around1092 and 854 cm^{-1} show asymmetric and symmetric of SiO_2 respectively. The strong peak in 469cm^{-1} are attributed to O-Si-O bond that exist in two graphs [33].

CONCLUSION

In this research, iron oxide- silica aerogel nanocomposites were synthesized successfully by sodium silicate precursor and ambient pressure drying method. Co-gelation of the nanoparticles and the matrix precursor were used to synthesize nanocomposites. The effect of two modification agents (HMDZ and TMCS) and the iron oxide content were investigated on the nanocomposite properties. The BET, AAS, SEM, TEM, VSM, FTIR and XRD method were used to characterize the result structures. HMDZ modified the gels without any effect on iron oxide nanoparticles and these particles retained their magnetic properties. By increasing the iron content of the samples, the density and specific surface area were increased. The minimum density of the synthesized samples by HMDZ in this research were 0.485g/cm^3 and the maximum specific surface area were 494.7m^2/g. The other analysis revealed the formation of porous magnetic silica aerogel. These structures can have many applications such as chemical and biochemical catalysts.

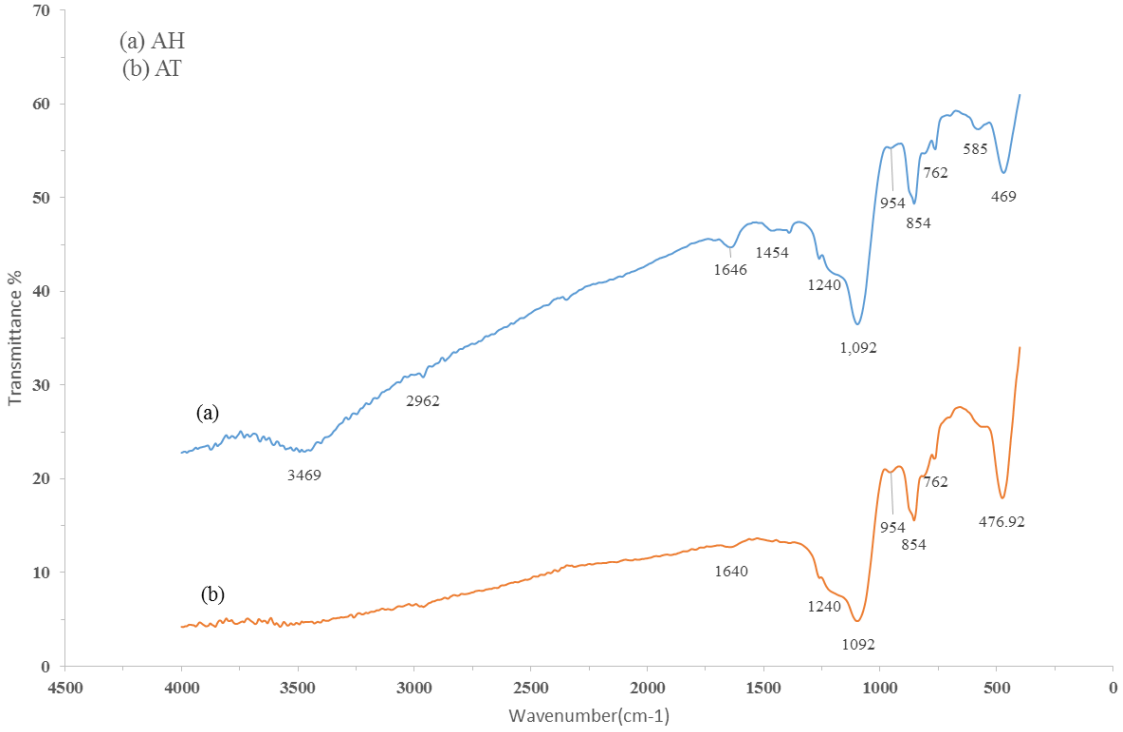

Fig. 9. FTIR spectra of (a) sample AH and (b) sample AT.

REFFERENCES

1. S. Santra, R. Tapec, N. Theodoropoulou, J. Dobson, A. Hebard, W. Tan, *Langmuir*, **17**, 2900 (2001).
2. S.P. Gubin, Y.A. Koksharov, G.B. Khomutov, G.Y. Yurkov, *Russ. Chem. Rev*., **74**, 489 (2005).
3. C. Cannas, M. F. Casula, G. Concas, A. Corrias, D. Gatteschi, A. Falqui, A. Musinu, C. Sangregorioc, G. Spano, *J. Mater. Chem.*, **11**, 180 (2001).
4. A.-H. Lu, E.L. Salabas, F. Schuth, *Angew. Chem. Int. Edit.*, 46, 1222 (2007).
5. M.E. Khosroshahi, L. Ghazanfari, M. Tahriri, *J. Exp. Nanosci.*, **6**, 580 **(2011).**
6. L. Casas, A. Roig, E. Rodriguez, E. Molins, J. Tejada, J. Sort, *J. Non-Cryst. Solids*, **285**, 37 (2001).
7. P.M. Zelis, M.B.F. van Raap, L.M. Socolovsky, A.G. Leyva, F.H. Sanchez, *Physica B*, **407**, 3113 (2012).
8. A.S. Dorcheh, M.H. Abbasi, *J. Mater. Process. Tech.*, **199**, 10 (2008).
9. F. Schwertfeger, D. Frank, M. Schmidt, *J. Non-Cryst. Solids*, **225**, 24 (1998).
10. F. Blanchard, B. Pommier, J.P. Reymond, S.J. Teichner, *Stud. Surf. Sci. Catal.*, **16**,395 (1983).
11. M. Soufyani, D. Bourret, A. Sivade, R. empere, *J. Non-Cryst. Solids*, **145**, 60 (1992).
12. M.R. Ayres, X.Y. Song, A.J. Hunt, *J. Mater. Sci.*, **31**, 6251 (1996).
13. C.T. Wang, R.J. Willey, *J. Non-Cryst. Solids*, **225**,173 (1998).
14. M.F. Casula, A. Corrias, G. Paschina, *J. Non-Cryst. Solids*, 25, 293 (2001**)**.
15. P. Fabrizioli, T. Burgi, A. Baiker, *J. Catal.*, **206**, 143 (2002).
16. M.B.F. van Raap, F.H. Sanchez, R.C.E. Torres, L. Casas, A. Roig, E. Molins, *J. Phys-Condens Mat.*, **17**, 6519 (2005**)**.
17. B.J. Clapsaddle, A.E. Gash, J.H.Jr. Satcher, R.L.Simpson, *J. Non-Cryst. Solids*, **331**, 190 (2003**)**.
18. S. Martinez, M. Meseguer, L. Casas, E. Rodriguez, E. Molins, M. Moreno-Manas, A. Roig, R.M. Sebastian, A. Vallribera, *Tetrahedron*, **59**, 1553 (2003).
19. M. Popovici, M. Gich, A. Roig, L. Casas, E. Molins, C. Savii, D. Becherescu, J. Sort, S. Surinach, J.S. Munoz, M. Dolors Baro, J. Nogues, *Langmuir*, **20,** 1425 (2004).
20. A. Lancok, K. Zaveta, M. Popovici, C. Savii, M. Gich, A. Roig, E. Molins, K. Barcova, *Hyperfine Interact*., **165**, 203 (2006).
21. K. Racka, M. Gich, A. Slawska-Waniewska, A. Roig, E. Molins, *J. Magn. Magn. Mater*., **127**, 290 (2005).
22. S. Masoudian, Hosseini H. Monfared, A. Aghaei, *Transition Met. Chem.*, **36**, 521 (2011). DOI 10.1007/s11243-011-9498-7.
23. C.T. Wang, R.J. Willey, *Catal. Today*, **52**, 83 (1999).
24. C.T. Wang, R.J. Willey, *J. Catal*., **202**, 211 (2001).
25. M.B.F. van Raap, F.H. Sanchez, A.G. Leyva, M.L. Japas, E. Cabanillas, H. Troiani, *PhysicaB*, **398**, 229 (2007).
26. H. Bargozin, L. Amirkhani, J.S. Moghaddas, M.M. Ahadian, *Sci Iran*, **17**, 122 (2010).
27. U.K.H. Bangi, A.V. Rao, A.P. Rao, *Sci. Technol. Adv. Mater*., **9**, 1 (2008). DOI 10.1088/1468-6996/9/3/035006
28. W.F. Kladnig, *J. Iron Steel Res. Int.*, **15**, 1 (2008).
29. A.P. Rao, A.V. Rao, G.M. Pajonk, P.M. Shewale, *J. Mater. Sci*., **42**, 8418 (2007).
30. H.P. Klug, , L.E. Alexender, X-ray Diffraction, Wiley, New York, 1974, 132
31. H. Xu, N. Tong, L. Cui, Y. Lu, H. Gu, *J. Magn. Magn. Mater***, 311**, 125 (2007).
32. K. Khoshnevisan, M. Barkhi, D. Zare, D. Davoodi, M. Tabatabaei, *Synth. React. Inorg. M.*, **42**, 644 (2012).
33. R. Al-Oweini, H. El-Rassy, *J. Mol. Struct*., **919**, 140 (2009**)**.